Applied Surface Science 702 (2025) 163356

Contents lists available at ScienceDirect

Applied Surface Science

journal homepage: www.elsevier.com/locate/apsusc

Full Length Article

Greatly enhanced exciton-photon coupling in a WS_2-Si_3N_4 nanohole array-Ag film heterostructure

Shulei Li [a], Fu Deng [b,*], Lujun Huang [c,*], Yatao Zhang [a], Lidan Zhou [d], Sheng Lan [b,*]

[a] School of Optoelectronic Engineering, Guangdong Polytechnic Normal University, Guangzhou 510665, China
[b] Guangdong Provincial Key Laboratory of Nanophotonic Functional Materials and Devices, School of Optoelectronic Science and Engineering, South China Normal University, Guangzhou 510006, China
[c] School of Physics and Electronic Science, East China Normal University, Shanghai 200241, China
[d] State Key Laboratory of Optoelectronic Materials and Technologies and School of Electronics and Information Technology, Sun Yat-sen University, Guangzhou 51006, China

ARTICLE INFO

Keywords:
Two-dimensional materials
Strong coupling
Surface lattice resonances
Excitons

ABSTRACT

Two-dimensional transition metal dichalcogenides (TMD) monolayers are recognized as a promising platform for realizing strong coupling due to their exceptionally large binding energies of excitons. Various types of optical resonances, including DBR-based Fabry-Perot resonances, plasmonic resonances, Mie resonances, and guided mode resonances, have been proposed to facilitate strong coupling between excitons in TMD monolayers and optical nanocavities. However, there has been limited research on the strong coupling between multiple resonances and excitons in TMD monolayers. In this study, we propose a heterostructure composed of a WS_2-Si_3N_4 nanohole array and an Ag film to achieve robust strong coupling among surface transverse waveguide modes, surface lattice resonances (or guided mode resonances), and excitons in a WS_2 monolayer. Such a hybrid heterostructure inherits both advantages of surface lattice resonances in a Si_3N_4 photonic crystal slab with the surface plasmon-like modes at the dielectric-Ag interface, resulting in low-loss optical resonances and excellent field confinement. Consequently, the light-matter interaction among the surface transverse waveguide mode, surface lattice resonances, and excitons in the WS_2 monolayer is significantly enhanced. Utilizing angle-resolved scattering spectra measurements and numerical simulations, we observe substantial Rabi splitting and shifts in resonant peaks, which are indicative of hybrid mode coupling. The experimental results closely align with the simulations, thereby confirming the hybrid coupling of the surface transverse waveguide mode, surface lattice resonances, and excitons. Notably, we show that Rabi splitting, an indicator of the coupling strength, is significantly increased to 318 meV, thereby entering the strong coupling regime within a three-oscillator framework. These results not only deepen the understanding of hybrid mode interactions within dielectric photonic structures but also promote advancements in high-performance optoelectronic applications.

1. Introduction

The two-dimensional (2D) transition metal dichalcogenides (TMD) have received tremendous attention due to their superior electronic and optical properties [1–3]. Notably, they are evolved from indirect bandgap semiconductors to direct bandgap semiconductors as the layer number is decreased from multilayers to monolayer limit, thereby enabling large quantum yields and giving rising to a remarkable photoluminescence (PL) in TMD monolayer [4]. On the other hand, the exciton resonance that dominates the PL spectrum has an exceptionally large binding energy [5]. This renders them an ideal candidate of studying strong coupling of exciton–polariton [3,6]. When TMD monolayers are integrated with different types of resonant nanostructures, strong light-matter interactions between optical resonances and exciton resonances in TMD monolayer can be induced [7–10], thus promising many interesting applications in quantum manipulation [11], ultrafast switching [12], and low-threshold lasers [13].

The phenomenon of strong coupling between optical resonances and excitons in monolayer TMD has garnered significant attention and has been successfully demonstrated across a variety of optical cavities, ranging from individual nanocavities to planar optical microcavities at ambient temperature [14–16]. At the level of single nanoparticles,

* Corresponding authors.
E-mail addresses: fu_deng@foxmail.com (F. Deng), ljhuang@phy.ecnu.edu.cn (L. Huang), slan@scnu.edu.cn (S. Lan).

https://doi.org/10.1016/j.apsusc.2025.163356
Received 7 October 2024; Received in revised form 16 February 2025; Accepted 24 April 2025
Available online 26 April 2025
0169-4332/© 2025 Elsevier B.V. All rights are reserved, including those for text and data mining, AI training, and similar technologies.

strong plasmon-exciton coupling has been achieved due to excellent field localization at the surface of nanoparticles, yielding a Rabi splitting in the range of 80–120 meV [17–19]. This coupling can be further improved in nanoparticle-on-film configurations that incorporate embedded monolayer TMD, resulting in Rabi splitting values of 120–170 meV [20,21]. Furthermore, when TMD are integrated with periodic structures, the Rabi splitting of the hybrid system can exceed 300 meV [22], and in the ultra-strong coupling regime, values surpassing 600 meV have been reported through the utilization of random metallic multi-singular nanostructures [23].

Except for plasmonic nanocavities, dielectric nanostructures have emerged as an alternative platform to enhance light-matter interactions with TMD [24–27]. Similar to the metallic nanostructure, all-dielectric structures support multipolar electric and magnetic Mie resonances. Comparing to plasmonic resonances, dielectric nanostructures have much lower loss, thus providing an alternative pathway for achieving strong coupling [28]. For instance, both theoretical and experimental investigations have suggested enhanced strong coupling of excitons in TMD with dielectric metasurfaces that support high-quality (high-Q) modes [29–33]. The interaction between excitons in WS_2 and Si_3N_4-based photonic crystals has been successfully demonstrated at low temperatures [34], while the strong coupling of discrete excitons in WS_2 monolayers with surface-transverse-waveguide mode in Si_3N_4-based slabs has been introduced at room temperature [35]. Despite tremendous progress made in the past few years, the Rabi splitting observed in such systems remains relatively modest, primarily due to the inherent limitations in field enhancement associated with dielectric nanostructures [36]. To mitigate this constraint, alternative strategies have been explored, one of which involves the hybridization of multiple resonances with excitons, significantly enhancing the Rabi splitting within the hybrid system [26,37,38]. This approach capitalizes on the synergistic effects of various resonant modes to amplify light-matter interactions, thereby presenting a novel avenue for achieving stronger coupling. Numerous studies have concentrated on micro- and nanocavities that facilitate three-dimensional confinement of light. Additionally, the intricate mutual coupling among multiple resonances complicates the direct and intuitive comprehension of exciton-photon coupling. In a prior investigation, we demonstrated that a dielectric-metal heterostructure can support transverse electric (TE) polarized surface waves that are confined to the surface of the Si_3N_4-Ag heterostructure [39], which we refer to as surface transverse waveguide modes (STWMs). The STWM exhibits a significantly enhanced factor for the in-plane electric field, suggesting a more robust interaction with the two-dimensional material integrated within the heterostructure. The optical characteristics of surface lattice resonances (SLR), including mode volume, dispersion, and linewidth, can be independently modified through geometric design, thereby offering a distinctive opportunity to tailor exciton-photon coupling [2]. In two-dimensional systems, SLR and STWM present an excellent platform for the investigation and manipulation of exciton-photon interactions due to their geometric compatibility.

In this study, we propose a hybrid WS_2-Si_3N_4 photonic crystal slab-Ag film structure, to promote strong coupling among various resonant modes. Such a hybrid heterostructure combines the advantage of low loss surface lattice resonances and extreme field confinement at the interface of dielectric-Ag film, thus significantly enhancing light-matter interactions. By utilizing the remarkable excitonic properties of WS_2 monolayers in combination with the SLR of a Si_3N_4 nanohole array sit on an Ag film-SiO_2 substrate, we aim to investigate the hybrid coupling of STWM, SLR, and excitons. Our approach includes both extensive numerical simulations and angle-resolved scattering spectra measurements to elucidate the dynamics of coupling and mode interactions within this hybrid system. The results indicate significant energy splitting and shifts in resonant peaks, which serve as evidence of effective hybrid mode coupling. Notably, we observe an enhanced Rabi splitting of 318 meV, highlighting the existence of strong coupling within a hybrid three-oscillator framework.

2. Materials and methods

2.1. Sample preparation and characterization

An Ag film with a thickness of 50 nm was deposited onto a silicon dioxide (SiO_2) substrate using electron beam evaporation. Subsequently, a silicon nitride (Si_3N_4) layer was applied over the Ag film through high-frequency plasma-enhanced chemical vapor deposition (HF-PECVD), utilizing a precursor gas mixture of SiH_4 and NH_3. The flow rates for SiH_4 and NH_3 were maintained at 3 sccm and 7.5 sccm, respectively. The radio frequency (RF) power, deposition pressure, and substrate temperature were set at 30 W, 60 Pa, and 80 °C, respectively. The Si_3N_4 layer with a thickness of 100 nm was achieved based on the deposition duration, and its optical constants were assessed using ellipsometry. Nanohole array with a hole diameter of 300 nm and a period of 500 nm within the Si_3N_4 layer were fabricated through electron beam lithography (EBL) and reactive ion etching (RIE). WS_2 monolayers were initially synthesized on a 300 nm SiO_2-Si substrate utilizing Chemical Vapor Deposition (CVD) techniques. A quantity of 1 mg of WO_3 was positioned on the substrate, with a blank wafer placed face-down approximately 2 to 3 mm above it. This assembly was subsequently enclosed within a pre-cleaned quartz tube, with 100 mg of sulfur positioned upstream, all within a larger tube furnace. The temperature gradually increased to 550 °C at a rate of 20 °C/min, followed by a further increase to 750 °C at a rate of 3 °C/min, where it was maintained for 5 min before allowing for natural cooling. The growth process was conducted under an argon flow of 100 sccm, resulting in the formation of triangular WS_2 monolayers. The WS_2 monolayer was then wet-transferred onto the nanoholes in the Si_3N_4 layer, effectively covering them [35]. The suspended 1L WS_2 subsequently disintegrated, forming a nanoporous WS_2 film. The morphology and composition of the nanoholes were further examined using a scanning electron microscope (SEM) (Gemini 500, Zeiss).

2.2. Optical characterization

The Kretschmann-Raether configuration is utilized to stimulate STWM in Si_3N_4-Ag and WS_2-Si_3N_4-Ag heterostructures, as illustrated in Fig. 1a. To activate the surface waveguide mode, *s*-polarized white light is introduced into the heterostructures through total internal reflection at the prism's surface. This occurs when the angle of incidence surpasses the critical angle (i.e., $\theta > \theta_c \approx 43°$). The white light source utilized in this study is produced by a halogen lamp (OSRAM, 12 V/100 W). The scattered light from the nanohole is then collected using a 50 × objective lens attached to an inverted microscope (Axio Observer A1, Zeiss) and directed to a spectrometer (SR-500i-B1, Andor) for spectral analysis or to a color charge-coupled device (DS-Ri2, Nikon) for imaging purposes.

2.3. Numerical simulation

The numerical analysis of the reflectance spectra for planar Si_3N_4-Ag film heterostructures and the scattering spectra of the nanohole array in Si_3N_4-Ag film and WS_2-Si_3N_4-Ag film heterostructures was conducted using the finite-difference time-domain (FDTD) method (Lumerical FDTD, https://www.lumerical.com). For regular arrays of nanoholes with varying periods, periodic boundary conditions were implemented in the lateral directions (x and y directions). The refractive index of Si_3N_4 was based on measured data, while the dielectric constants of Ag and WS_2 monolayers were obtained from the literature [40,41]. The resonant energy of excitons in the WS_2 monolayer was determined to be 2.01 eV. The thicknesses of the WS_2, Si_3N_4, and Ag layers were set to 1.0 nm, 90 nm, and 50 nm, respectively. To ensure converged simulation results, the smallest mesh size was set to 0.5 nm.

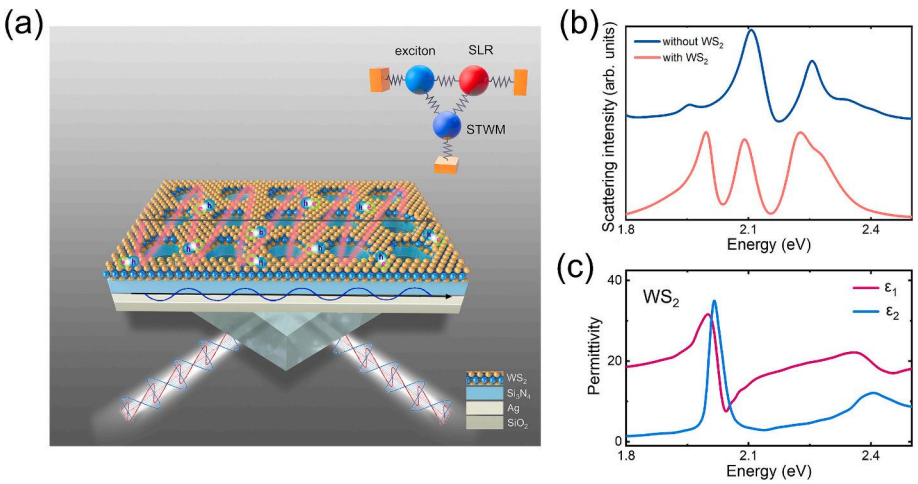

Fig. 1. (a) Schematic illustrating the excitation of a WS_2-Si_3N_4 nanohole array-Ag film heterostructure using prism-coupled STWM. The inset shows the strong coupling among the three oscillators: STWM, SLR, and excitons. (b) Scattering spectra of the nanohole cavity without the WS_2 monolayer (blue) and with the WS_2 monolayer (red). (c) Complex permittivity of the WS_2 monolayer used in the simulations. ε_1 and ε_2 represent the real and imaginary parts of the permittivity, respectively. (For interpretation of the references to color in this figure legend, the reader is referred to the web version of this article.)

3. Results and discussion

To introduce hybrid coupling in dielectric photonic structures with TMD monolayers, we utilize the hybrid system shown in Fig. 1a. This system comprises a WS_2-Si_3N_4 nanohole array placed on an Ag film (50 nm)-SiO_2 substrate. The structure is illuminated using a prism-coupled white light source to excite hybrid modes of the systems, including STWM and SLR supported by the Si_3N_4 nanohole array-Ag film heterostructure. STWM with strong field enhancement and low radiation loss is generated at the interface of a dielectric slab coated on a metallic film. This phenomenon is analogous to surface plasmon polaritons observed at a dielectric-metal interface; however, it is excited by a TE-polarized wave and exhibits reduced radiation loss, as detailed in prior studies [35,39,42]. Since STWM cannot be generated directly at the dielectric-air interface, a prism is used to couple the light with matching momentum to excite the STWM and the dispersion of the STWM can be changed via the incident angle (Fig. S1). Additionally, the prism-coupled illumination method provides an easy way to change the incident angle of the white light in our setup, allowing us to introduce the angle-resolve spectra results in the following. It is important to note that such a structure can also be studied using common reflectance/transmittance spectra measurement, which can yield similar results. However, incorporating this method into our system is not as straightforward, so we focus mainly on the scattering spectra for collaboration with experimental demonstration.

Introducing a periodic nanohole structure in the dielectric slab generates a new mode from the SLR [43], which couples with the STWM of the pure slab. This coupling is confirmed by the scattering spectra shown in Fig. 1b, where the two-mode coupling causes the spectra to split into two new hybrid modes. It has been observed that the spectrum contains two supplementary peaks characterized by weak resonances, which may be attributed to higher-order SLR. These peaks do not demonstrate substantial field confinement or significant overlap with the exciton of WS_2. Consequently, they do not play a meaningful role in the hybrid coupling mechanism being examined. Thus, the subsequent discussion will concentrate on the two primary resonances, which are essential to the strong coupling process. By incorporating a WS_2 monolayer into the system, which supports strong excitonic responses in the visible range (as indicated by the dielectric function in Fig. 1c), hybrid coupling between STWM, SLR, and excitons can be realized. This coupling is further confirmed by the mode splitting observed in Fig. 1b. More details on the hybrid system will be provided from both simulation and experimental perspectives in the following sections. In the context of lattice resonance modes within periodic structures, the composition and dispersion of polaritons are typically adjusted by modifying the geometries of nanoparticles and lattices. This approach facilitates the design of various properties within the system and enables the coexistence of multiple resonances characterized by distinct physical properties. This study demonstrates the strong coupling between STWM waves and excitons in the WS_2 monolayer. Furthermore, introducing a new resonance mode, such as SLR, can prolong the oscillation time of the resonance mode and yield substantial Rabi splitting energy. Here, the interaction between SLR, induced by nanohole arrays, and STWM waves, in conjunction with the localized electric field intensity of a dielectric film surface, results in a significantly higher Rabi splitting energy compared to STWM and WS_2 excitons in isolation.

Fig. 2a presents the simulated two-dimensional scattering spectra (color map) for the base Si_3N_4 nanohole array structure illuminated by the prism-coupled light source at varying incident angles. A prominent anti-crossing behavior is observed, indicating the strong coupling between the STWM and SLR modes. As discussed previously, the STWM mode changes significantly with varying incident angles, while the SLR mode remains nearly constant in wavelength, facilitating the anti-crossing behavior. To confirm that the observed coupling arises from the interaction of STWM and SLR modes, we examine the electric field distribution in the X-Z and X-Y planes of the upper polariton (UP) band with the wavelength of 540 nm at zero detuning angle (49°), as shown in Fig. 2b and 2c. These distributions demonstrate contributions from both coupled modes. The electric field is mainly confined to the surface and corners of the remaining Si_3N_4 structure, indicating that the light fields of the two modes interact at the surface. In the top view of the electric field in Fig. 2c, the field is distributed on both sides of the hole, confirming the contribution from the SLR mode originating from the periodical structure.

To quantitatively characterize the coupling between the STWM and SLR modes in the Si_3N_4 hole system, the widely used coupled oscillator model (COM) with two oscillators is adopted to understand the coupling system [44,45]:

$$\begin{pmatrix} E_{STWM} - i\frac{\gamma_{STWM}}{2} & g \\ g & E_{SLR} - i\frac{\gamma_{SLR}}{2} \end{pmatrix} \begin{pmatrix} \alpha \\ \beta \end{pmatrix} = E_{\pm} \begin{pmatrix} \alpha \\ \beta \end{pmatrix} \quad (1)$$

where E_{STWM} and E_{SLR} are the resonant energies of the STWM and SLR, γ_{STWM}, and γ_{SLR} are the corresponding damping rates, g is the coupling strength between the two oscillators, $E_{\pm}$ are the eigenenergies of the

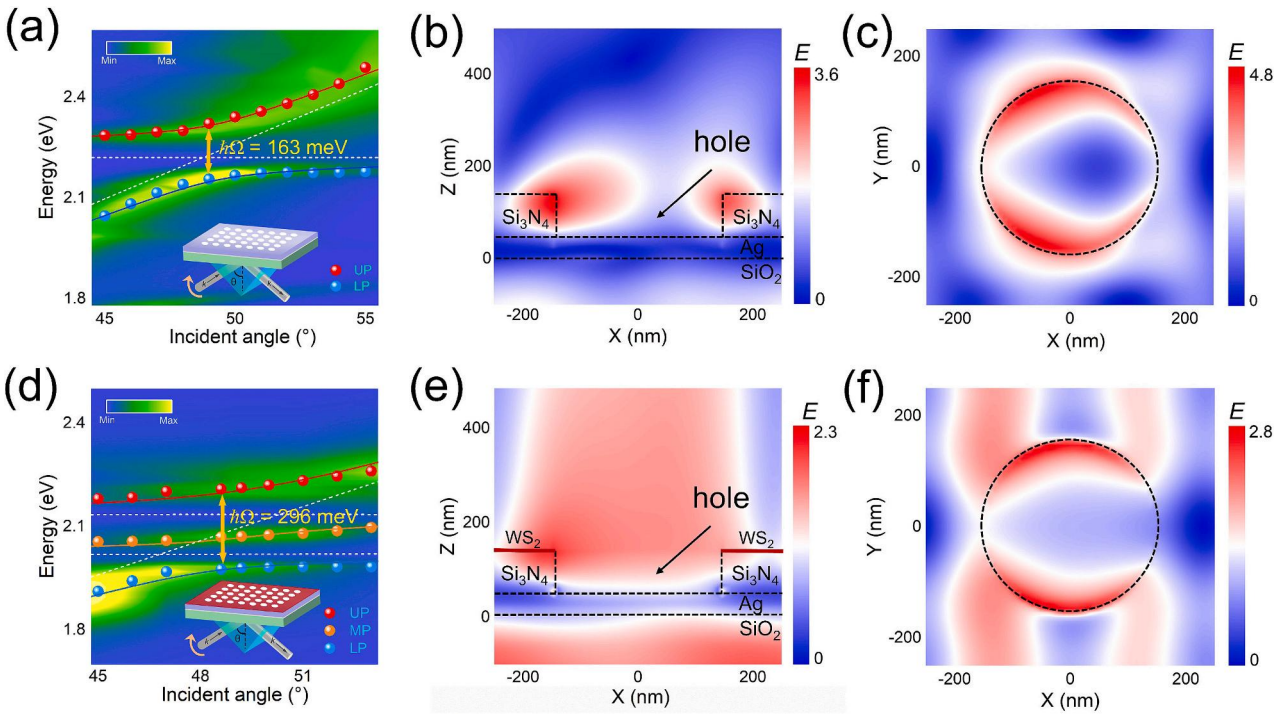

Fig. 2. (a) Evolution of the scattering spectra of the Si_3N_4 nanohole array structure with varying incident angles in simulation (color map). The solid lines represent the fitting using COM with two coupled oscillators. The dashed lines denote the uncoupled STWM and SLR modes, respectively. (b), (c) Electric field distribution of the designed structure in the X-Z plane (b) and X-Y plane (c) at the wavelength of 540 nm. (d) Evolution of the scattering spectra of the WS_2-Si_3N_4 nanohole array-Ag film heterostructure with varying incident angles in simulation (color map). The lines represent the fitting using COM with three coupled oscillators. The dashed lines denote the uncoupled excitons, STWM, and SLR modes, respectively. (e), (f) Electric field distribution of the designed structure in the X-Z plane (e) and X-Y plane (f) at the wavelength of the UP at zero detuning.

hybrid states, and α and β are the eigenvectors satisfying $|\alpha|^2 + |\beta|^2 = 1$ (Fig. S2). The eigenenergies $E_\pm$ can be derived as follows [19,46]:

$$E_\pm = \frac{E_{STWM} + E_{SLR}}{2} \pm \frac{\sqrt{4g^2 + (\delta - \frac{i}{2}(\gamma_{STWM} - \gamma_{SLR}))^2}}{2} \quad (2)$$

where $\delta = E_{STWM} - E_{SLR}$ is the detuning energy of the two resonances. The Rabi splitting energy can be obtained at zero detuning energy of $E_{STWM} = E_{SLR}$:

$$\hbar\Omega = \sqrt{4g^2 - \frac{(\gamma_{STWM} - \gamma_{SLR})^2}{4}} \quad (3)$$

The values of damping rates γ_{STWM} and γ_{SLR} can be extracted from simulation spectra. There are two criteria for strong coupling, the first one is the appearance of anti-crossing behavior in the energy diagram, as shown in Fig. 2a. The second is that energy splitting should satisfy the condition of $\hbar\Omega > (\gamma_{STWM} + \gamma_{SLR})/2$ [47]. The fitting results by COM with coupling strength $g = 81.5$ meV are shown in Fig. 2a as the solid lines with the coupling between the STWM and SLR modes in the system. In this case, Rabi splitting is obtained as $\hbar\Omega = 163$ meV from the fitting results at the incident angle of zero detuning. The damping rate of STWM in the fitting process is derived from the reflection spectra of the Si_3N_4–Ag film heterostructure, as $\gamma_{STWM} = 44$ meV, which was elaborated upon in our prior research [35]. Additionally, the damping rate of SLR is obtained as $\gamma_{SLR} = 165$ meV through the fitting of the angle-resolved spectra presented in Fig. 2a. Thus, the second criterion for the strong coupling condition is satisfied in our simulation, meaning the coupling between STWM and SLR of Si_3N_4 nanohole enters the strong coupling region.

Since the electric field distribution of the coupled STWM and SLR system is confirmed to be confined at the surface of the structure, this offers an opportunity to enhance interaction with monolayer 2D materials. Therefore, we investigate the hybrid nanohole system composed of a Si_3N_4 nanohole array with a WS_2 monolayer, as shown in Fig. 2d. The inherent thinness of the WS_2 monolayer renders it vulnerable to collapse when positioned on the nanopore of the Si_3N_4 array. We performed a comparative analysis of the strong coupling characteristics between the collapsed and non-collapsed WS_2 monolayers located on the nanopore (refer to Fig. S3). Notably, the Rabi splitting energy associated with the hybrid mode of strong coupling appears to be only marginally affected by the state of the WS_2 monolayer, regardless of whether it is collapsed or non-collapsed. Interestingly, the collapsed WS_2 monolayer demonstrates a slightly larger Rabi splitting energy. Consequently, the hybrid coupling of STEW, SLR, and excitons can also be incorporated into the structure featuring a non-collapsed monolayer of WS_2 on the Si_3N_4 nanohole array. In light of the considerations regarding the practicality of preparation and optical losses, lattice parameters were chosen to position the SLR mode at approximately 2.1 eV. The minor detuning between the SLR and the excitonic state of WS_2 contributes to a reduction in non-radiative losses, while also alleviating broadening effects. This detuning further enables hybridization with other optical modes present in the system, thereby optimizing field constraints and enhancing interaction strength.

The simulated 2D scattering spectra demonstrate that the coupled STWM and SLR modes interact with the excitons of the WS_2 monolayer, leading to the formation of three hybrid states—upper polariton (UP), middle polariton (MP), and lower polariton (LP)—in the scattering spectra as the incident angle varies. The coupling of the three modes is quantitatively characterized by using the COM but with three oscillators rather than two oscillators in the bare Si_3N_4 nanohole structure [37,48]:

$$\hat{H} = \hbar \begin{pmatrix} E_{STWM} - i\frac{\gamma_{STWM}}{2} & g_{STWM-ex} & g_{STWM-SLR} \\ g_{STWM-ex} & E_{SLR} - i\frac{\gamma_{ex}}{2} & g_{SLR-ex} \\ g_{STWM-SLR} & g_{SLR-ex} & E_{ex} - i\frac{\gamma_{SLR}}{2} \end{pmatrix} \quad (4)$$

where E_{STWM}, E_{SLR}, and E_{ex} are the resonant energies of the uncoupled STWM, SLR, and exciton, respectively. γ_{STWM}, γ_{SLR}, and γ_{ex} denote the corresponding dissipation rates of different modes. $g_{STWM-SLR}$, $g_{STWM-ex}$, and g_{SLR-ex} represent the coupling strengths between the STWM and the SLR, that between the STWM and the exciton, and that between the SLR and exciton, respectively.

By fitting the angle-resolved spectra from simulation by using Eq. (4), the dispersion and coupling strength of different resonances can be extracted. It is noted that the coupling strength between optical resonance modes and excitons in the system depends on several key parameters. These include the exciton oscillator strength, which determines the interaction efficiency, and the spectral overlap between excitonic and optical resonances, ensuring efficient energy exchange. Additionally, the quality factor of the resonant modes influences the field confinement. The fitted dispersion curves of the hybrid polaritons are shown in Fig. 2d, with blue, orange, and red solid lines representing the LP, MP, and UP, respectively. In this case, the coupling strengths between different modes are obtained to be $g_{STWM-SLR}$ = 88 meV, $g_{STWM-ex}$ = 61 meV, and g_{SLR-ex} = 70 meV, respectively. It is noted that the coupled strength between STWM and SLR is slightly larger than that of the case without WS_2 upon, which can be explained as follows. The presence of excitons facilitates the interaction between the STWM and the SLR. In the coupling of these three modes, excitons contribute additional hybridization pathways, thereby augmenting the coupling between STWM and SLR. Consequently, this phenomenon illustrates an enhanced strong coupling between light and excitons through the incorporation of a hybrid structure that couples STWM and SLR. The energy splitting (Rabi splitting) of $\hbar\Omega \approx 296$ meV obtained at zero detuning angle 49° in our simulation confirms this enhancement. The increased coupling with the WS_2 monolayer is further validated by the electric field distribution in Fig. 2e and 2f, where the electric field extends into the WS_2 area rather than being confined only to the sides of the nanohole. Our simulation suggests a method to achieve large energy splitting in the hybrid structure with a WS_2 monolayer, which will be further verified experimentally in the following sections. It is important to determine the coupling of the hybrid system, which obeys the criteria in a three-oscillator system [22]:

$$\hbar\Omega > W_{UP}\gamma_{UP} + W_{MP}\gamma_{MP} + W_{LP}\gamma_{LP} \quad (5)$$

where W_{UP}, W_{MP}, and W_{LP} represent the weighting coefficients of UP, MP, and LP branches of the system, γ_{UP}, γ_{MP}, and γ_{LP} are the linewidths of the three hybrid branches (Fig. S4), respectively. In our case, the strong coupling criteria for the STWM, the exciton, and the SLR modes can be derived (see Supporting Information Note 4):

$$\hbar\Omega > 41.4\%\gamma_{STWM} + 37.5\%\gamma_{ex} + 21.1\%\gamma_{SLR} \quad (6)$$

where γ_{STWM} = 40 meV, γ_{SLR} = 160 meV, and γ_{ex} = 33 meV are the corresponding linewidth of three oscillators. In this case, the criterion for strong coupling is satisfied with $\hbar\Omega \approx 296$ meV obtained from our simulation results, meaning the hybrid coupling of the system enters the strong coupling regions based on the simulation.

After organizing the results from simulations and COM of hybrid strong coupling in the system, we proceed to the experimental investigation of hybrid strong coupling in the hybrid WS_2-Si_3N_4 nanohole array structure. Fig. 3a illustrates the experimental setup of a custom-made angle-resolved scattering spectra measurement, and further details can

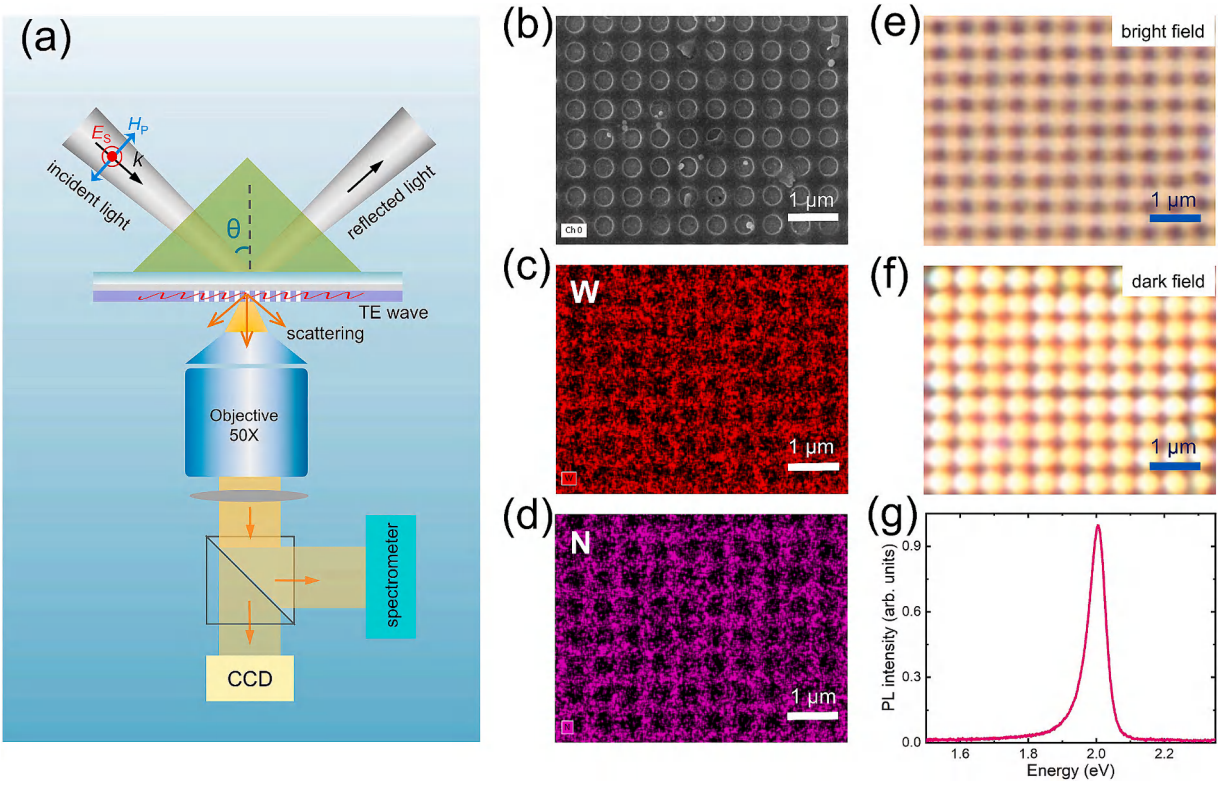

Fig. 3. (a) Schematic of the experimental configuration. A prism is used to couple the incident light into the hybrid system to excite the STWM. (b) SEM image of the hybrid nanohole structure. (c), (d) EDS images of the hybrid nanohole structure, confirming the presence of W atoms (c) and N atoms (d), respectively. The nanohole array with a diameter of 300 nm and a periodicity of 500 nm is fabricated. (e), (f) Optical images of the hybrid nanohole structure captured using bright-field microscopy (e) and dark-field microscopy (f). (g) PL spectrum of the WS_2 monolayer used in forming the hybrid nanohole structure.

be found in previous works [26,35,39]. It is noted that the system may be influenced by various parameters, including environmental temperature and humidity. Temperature has a significant impact on exciton binding energy, linewidth broadening, and resonance shifts in WS_2 monolayers. Elevated temperatures typically lead to a reduction in exciton binding energy and an increase in linewidth due to phonon interactions, which may compromise strong coupling [44]. However, the experiments were conducted in a controlled environment with regulated temperature and humidity, thereby minimizing external influences on the system. Consequently, the effects of environmental temperature and humidity can be considered negligible in the context of our experiment. For sample fabrication, a 90 nm thick Si_3N_4 slab was first deposited on an Ag film (50 nm)-SiO_2 substrate. Subsequently, a nanohole array with a diameter of 300 nm and a periodicity of 500 nm was fabricated on the Si_3N_4 slab. Finally, a CVD-grown WS_2 monolayer was transferred onto the well-fabricated nanohole structure to form the hybrid WS_2-Si_3N_4 nanohole array structure. The CVD-grown WS_2 monolayer was characterized using Raman spectroscopy, as shown in Fig. S5, and the results are consistent with existing literature [3]. After fabricating the hybrid structure, the sample was characterized using SEM and energy dispersive spectroscopy (EDS) measurements, as shown in Fig. 3b-d. The SEM image in Fig. 3b clearly shows the nanohole structure. It is noted that the WS_2 tends to break and fill into the hole structure due to strain, as confirmed by EDS measurements. The distribution of W atoms from the WS_2 monolayer is similar to that of N atoms from the Si_3N_4, indicating that the WS_2 monolayer conforms to the nanohole structure of Si_3N_4. Thus, we confirm the successful fabrication of the hybrid WS_2-Si_3N_4 nanohole structure in our experiments. To better illustrate the sample, optical images from bright-field and dark-field microscopies were taken, as shown in Fig. 3e and 3f, further confirming the fabricated structures. Another important factor is the quality of the WS_2 monolayer which may affect the measurements in the strong coupling experiment. Photoluminescence (PL) measurements were performed on the WS_2 monolayer sample, as shown in Fig. 3g. The PL spectrum shows a single peak around 2.05 eV with an FWHM of 50 meV, confirming the high quality of the WS_2 monolayer in the hybrid structure.

After fabricating and characterizing the hybrid WS_2-Si_3N_4 nanohole array-Ag film heterostructure, we performed experiments on the hybrid system. For the bare Si_3N_4 nanohole array structure, the angle-resolved scattering spectra are shown in Fig. 4a. Mode splitting behavior is observed in the scattering spectra, and the resonant frequencies blueshift with increasing incident angle. Numerical simulations, incorporating the true parameters from experimental data in Fig. 3, were conducted to match the experimental results. These simulations, shown in the right panel of Fig. 4a, agree well with the experimental results. It is noted that some small peaks appear in the spectra, particularly at small incident angles. These peaks are likely caused by higher-order lattice resonances in the periodic structure and do not significantly affect the main result of strong mode coupling. To quantitatively characterize the coupling between the STWM and SLR modes, we applied COM with two oscillators in Eq. (1) to fit the resonant peaks extracted from the experimental results (dashed curve in Fig. 4a). This fitting shows good agreement with the experimental results, as shown in Fig. 4b. The Rabi splitting, obtained from the fitting results, is 171 meV. Fig. 4c shows the fractions of STWM and SLR in the UP state within the coupled system, which results in the formation of hybrid polaritons characterized by energy transfer between the two phenomena. It is evident that the contributions of STWM and SLR become equal at zero detuning, each accounting for 50 %. This indicates that the UP exhibits properties that are equally derived from STWM and SLR, signifying a strong coupling between these two processes. The experimental findings indicate that the damping rate of the STWM is approximately 48 meV, while a value of around 170 meV is derived from the fitting of angle-resolved scattering spectra, which agrees with the simulation results. This

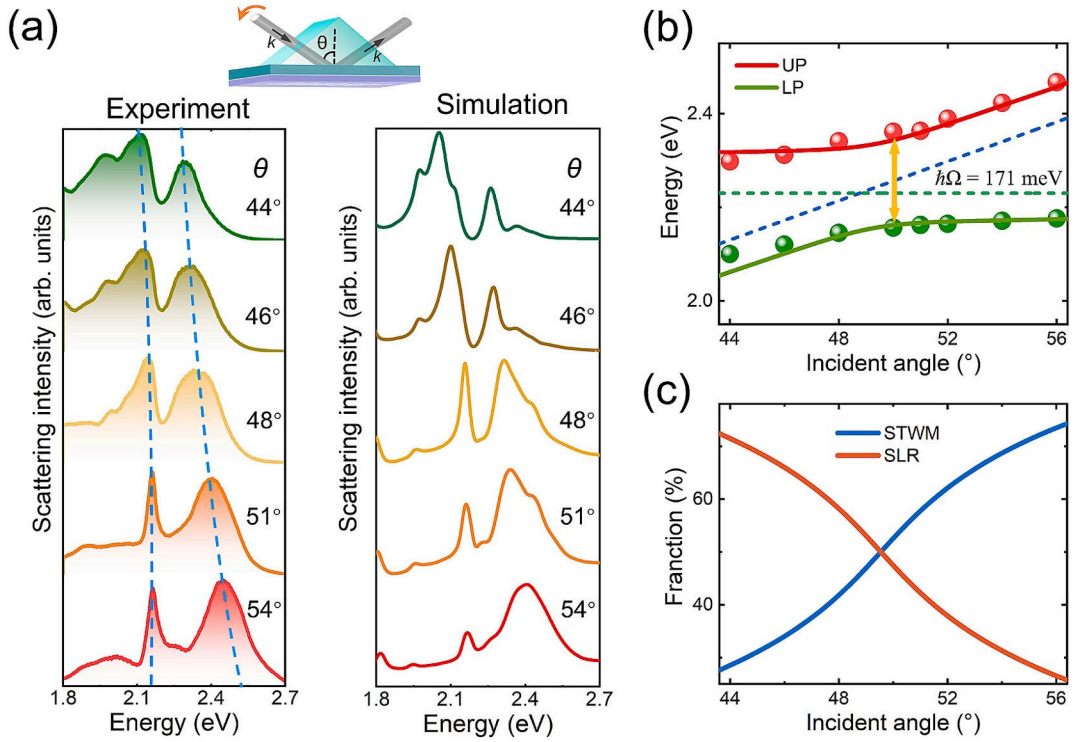

Fig. 4. (a) Experimental (left) and simulated (right) angle-dependent scattering spectra of the Si_3N_4 nanohole array on Ag film/SiO_2 structure. The upper structure shows the direction and method of excitation in the experiment. (b) Dispersion curves of the hybrid nanohole structure as a function of incident angle. Green and red spheres represent the resonant peaks extracted from the experimental spectra in (a). The solid lines are fitted using the COM with two oscillators. The dashed lines represent the uncoupled STWM and SLR modes, respectively. (c) Fractions of STWM and SLR in the UP state of the system. (For interpretation of the references to color in this figure legend, the reader is referred to the web version of this article.)

observation fulfills the criterion for strong coupling, suggesting that the interaction between the STWM and the SLR within the Si_3N_4 nanohole array has transitioned into the strong coupling regime.

Fig. 5 shows the experimental results of the angle-resolved scattering spectra for the WS_2-Si_3N_4 nanohole array-Ag film heterostructure, using the experimental setup illustrated in Fig. 3a. This hybrid system exhibits energy splitting in the scattering spectra, with three resonance peaks, as expected from the simulated results in Fig. 2. The resonances blue shift with increasing the incident angle, similar to the behavior observed experimentally in the bare Si_3N_4 nanohole array system shown in Fig. 4. Experimental results closely replicate the simulation results for the WS_2-Si_3N_4 nanohole array-Ag film heterostructure, confirming the hybrid STWM-SLR-exciton coupling in the system. It is observed that the spectra presented in Fig. 5a exhibits more than three modes, with the additional weak resonant peaks arising from fabrication imperfections in the etched nanohole array, which result in minor structural variations. The identification of pertinent optical modes was conducted through a synthesis of numerical simulations and angle-resolved scattering spectra. Our analysis concentrated on the modes that demonstrate strong coupling with excitons, as evidenced by their spectral positions, linewidths, and field distributions obtained from simulations. The weaker, unintended peaks exert a negligible influence on the hybrid coupling mechanism and do not substantially alter our conclusions. To further investigate the strong coupling in the system, the wavelengths of the resonant peaks were extracted and fitted using COM with three oscillators in Eq. (4), as shown in Fig. 5b. The Rabi splitting in the experimental results is enhanced to 318 meV compared to the system without WS_2 monolayers. Furthermore, Fig. 5c shows the fractions of three coupled modes in the MP state of the system, indicating the energy exchange among the different modes. It is evident that the exciton and SLR predominantly contribute to the MP state, and their contributions can vary with changes in the incident angle and wavelength. This variation ensures the energy exchange between different modes (refer to Supporting Information Note 4 for further details).

In the hybrid system exhibiting robust coupling among STWM, SLR, and excitons, experimental measurements have established an energy splitting of $\hbar\Omega = 318$ meV. The damping rates of the corresponding modes with $\gamma_{STWM} \approx 55$ meV, $\gamma_{SLR} \approx 170$ meV, and $\gamma_{ex} \approx 50$ meV fulfill the criteria for strong coupling in a three-oscillator framework, as delineated in Eq. (6). Consequently, it can be inferred that the interactions among STWM, SLR, and excitons within the WS_2-Si_3N_4 nanohole array-Ag film heterostructure are situated within the strong coupling regime. This observation signifies a notable enhancement in coupling strength relative to the STWM-exciton interactions observed in the absence of the nanohole architecture. It is also pertinent to mention that the detuning of resonances within the hybrid system is achieved by varying the incident angle during experimentation; alternatively, this can be accomplished by adjusting the period of the Si_3N_4 array to modify the resonance wavelength of the SLR mode (Fig. S6). Furthermore, we conducted numerical simulations by altering the polarization from s-polarization to p-polarization and examined the resultant scattering signals (see Supporting Information Note 7). Our findings indicate that transitioning to p-polarized light incidence leads to the absence of a discernible scattering signal. These results substantiate the notion that hybrid coupling can be effectively influenced by the incident polarization, aligning with our earlier observations. Moreover, it is crucial to recognize that the coupling strength may be further increased through the careful design of the nanohole structure, which could enable the incorporation of stronger resonances with high-quality factors, such as guided-mode resonances or bound states in the continuum (BIC) within dielectric structures [49].

4. Conclusions

In conclusion, we have successfully demonstrated a heterostructure comprising a WS_2-Si_3N_4 nanohole array and an Ag film, which exhibits

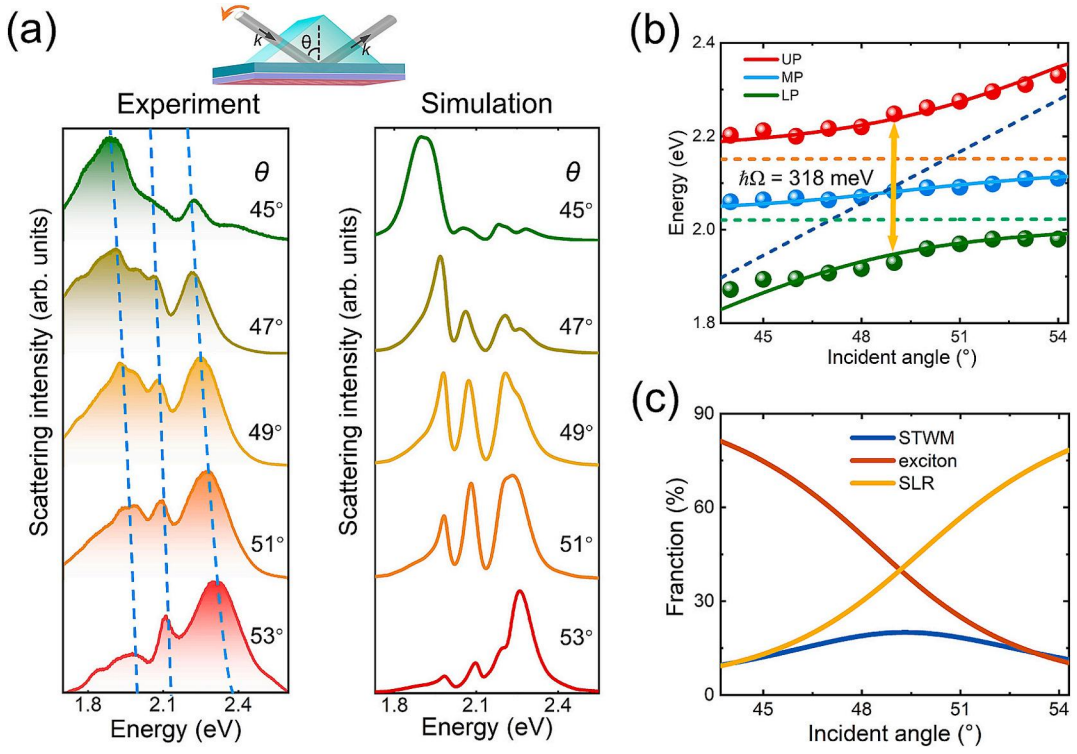

Fig. 5. (a) Experimental (left) and simulated (right) scattering spectra of the WS_2-Si_3N_4 nanohole array-Ag film heterostructure with various incident angles. The upper structure shows the direction and method of excitation in the experiment. (b) Dispersion curves of the hybrid nanohole structure as a function of incident angle. Colored spheres represent the resonant peaks extracted from the experimental spectra in (a). The solid lines are fitted using COM with three oscillators. The dashed lines represent the uncoupled STWM, exciton, and SLR modes, respectively. (c) Fractions of STWM, exciton, and SLR in the MP state of the system.

strong coupling between STWM, SLR, and excitons. Both experimental and simulation results indicate significant energy splitting in the scattering spectra, thereby confirming the presence of hybrid coupling within the system. The angle-resolved scattering spectra further revealed that the resonant peaks exhibit a blue shift with increasing incident angles, a behavior that aligns with that of the bare Si_3N_4 nanohole array-Ag film heterostructure. Our numerical simulations closely matched the experimental findings, thereby validating the existence of hybrid STWM-SLR-exciton coupling. The extracted resonant peaks, along with their fitting using COM with three oscillators, quantitatively assessed the coupling strength, revealing an enhanced Rabi splitting of 318 meV. The strong coupling criterion was fully satisfied in our hybrid system, demonstrating a significant enhancement compared to the STWM-exciton coupling observed in the absence of the nanohole structure. These findings represent a substantial advancement in the manipulation of hybrid modes within dielectric photonic structures integrated with TMD monolayers.

CRediT authorship contribution statement

Shulei Li: Writing – original draft, Validation, Investigation, Funding acquisition, Formal analysis, Data curation. **Fu Deng:** Writing – original draft, Validation, Methodology, Formal analysis, Data curation. **Lujun Huang:** Validation, Methodology, Funding acquisition, Formal analysis, Data curation. **Yatao Zhang:** Formal analysis. **Lidan Zhou:** Data curation. **Sheng Lan:** Writing – review & editing, Resources, Project administration, Methodology, Funding acquisition, Formal analysis.

Declaration of competing interest

The authors declare that they have no known competing financial interests or personal relationships that could have appeared to influence the work reported in this paper.

Acknowledgement

This work was financially supported by the National Natural Science Foundation of China (Grant Nos. 12174123, 12374347), Guangdong Basic and Applied Basic Research Foundation (Grant No. 2025A1515012291), Start-Up Funding of Guangdong Polytechnic Normal University (2022SDKYA007), and Shanghai Pujiang Program (22PJ1402900).

Appendix A. Supplementary material

Supplementary data to this article can be found online at https://doi.org/10.1016/j.apsusc.2025.163356.

Data availability

Data will be made available on request.

References

[1] L. Huang, A. Krasnok, A. Alú, Y. Yu, D. Neshev, A.E. Miroshnichenko, Enhanced light–matter interaction in two-dimensional transition metal dichalcogenides, Rep. Prog. Phys. 85 (2022) 046401.
[2] X. Ma, N. Youngblood, X. Liu, Y. Cheng, P. Cunha, K. Kudtarkar, X. Wang, S. Lan, Engineering photonic environments for two-dimensional materials, Nanophotonics 10 (2021) 1031–1058.
[3] S.B. Anantharaman, K. Jo, D. Jariwala, Exciton–photonics: from fundamental science to applications, ACS Nano 15 (2021) 12628–12654.
[4] G. Wang, A. Chernikov, M.M. Glazov, T.F. Heinz, X. Marie, T. Amand, B. Urbaszek, Colloquium: excitons in atomically thin transition metal dichalcogenides, Rev. Mod. Phys. 90 (2018) 021001.
[5] A. Chernikov, T.C. Berkelbach, H.M. Hill, A. Rigosi, Y. Li, B. Aslan, D.R. Reichman, M.S. Hybertsen, T.F. Heinz, Exciton binding energy and nonhydrogenic Rydberg series in monolayer WS_2, Phys. Rev. Lett. 113 (2014) 076802.
[6] R. Perea-Causin, D. Erkensten, J.M. Fitzgerald, J.J. Thompson, R. Rosati, S. Brem, E. Malic, Exciton optics, dynamics, and transport in atomically thin semiconductors, APL Mater. 10 (2022).
[7] X. Liu, T. Galfsky, Z. Sun, F. Xia, E.-C. Lin, Y.-H. Lee, S. Kéna-Cohen, V.M. Menon, Strong light–matter coupling in two-dimensional atomic crystals, Nat. Photonics 9 (2015) 30–34.
[8] J. Qin, Y.-H. Chen, Z. Zhang, Y. Zhang, R.J. Blaikie, B. Ding, M. Qiu, Revealing strong plasmon-exciton coupling between nanogap resonators and two-dimensional semiconductors at ambient conditions, Phys. Rev. Lett. 124 (2020) 063902.
[9] A.M. Berhe, K. As'ham, I. Al-Ani, H.T. Hattori, A.E. Miroshnichenko, Strong coupling and catenary field enhancement in the hybrid plasmonic metamaterial cavity and TMDC monolayers, Opto-Electronic Adv., 7 (2024) 230181-1-230181-13.
[10] Y. Chen, S. Miao, T. Wang, D. Zhong, A. Saxena, C. Chow, J. Whitehead, D. Gerace, X. Xu, S.-F. Shi, Metasurface integrated monolayer exciton polariton, Nano Lett. 20 (2020) 5292–5300.
[11] J.C. Thomas, W. Chen, Y. Xiong, B.A. Barker, J. Zhou, W. Chen, A. Rossi, N. Kelly, Z. Yu, D. Zhou, S. Kumari, E.S. Barnard, J.A. Robinson, M. Terrones, A. Schwartzberg, D.F. Ogletree, E. Rotenberg, M.M. Noack, S. Griffin, A. Raja, D. A. Strubbe, G.-M. Rignanese, A. Weber-Bargioni, G. Hautier, A substitutional quantum defect in WS2 discovered by high-throughput computational screening and fabricated by site-selective STM manipulation, Nat. Commun. 15 (2024) 3556.
[12] Y. Tang, Y. Zhang, H. Ouyang, M. Zhao, H. Hao, K. Wei, H. Li, Y. Sui, J. You, X. Zheng, Z. Xu, X. Cheng, L. Shi, T. Jiang, Ultrafast response of a hybrid device based on strongly coupled monolayer WS_2 and photonic crystals: the effect of photoinduced coulombic screening, Laser Photonics Rev. 14 (2020) 1900419.
[13] S. Liu, R. Lv, Y. Wang, J. Wang, Y. Wang, H. Wang, Passively mode-locked fiber laser with WS_2/SiO_2 saturable absorber fabricated by sol–gel technique, ACS Appl. Mater. Interfaces 12 (2020) 29625–29630.
[14] J. Zhong, J.-Y. Li, J. Liu, Y. Xiang, H. Feng, R. Liu, W. Li, X.-H. Wang, Room-temperature strong coupling of few-exciton in a monolayer WS_2 with plasmon and dispersion deviation, Nano Lett. 24 (2024) 1579–1586.
[15] C. Schneider, M.M. Glazov, T. Korn, S. Höfling, B. Urbaszek, Two-dimensional semiconductors in the regime of strong light-matter coupling, Nat. Commun. 9 (2018) 2695.
[16] N. Zorn Morales, D.S. Rühl, S. Sadofev, G. Ligorio, E. List-Kratochvil, G. Kewes, S. Blumstengel, Strong coupling of monolayer WS_2 excitons and surface plasmon polaritons in a planar Ag/WS_2 hybrid structure, Phys. Rev. B 108 (2023) 165426.
[17] Y. Jiang, H. Wang, S. Wen, H. Chen, S. Deng, Resonance coupling in an individual gold nanorod–monolayer WS_2 heterostructure: photoluminescence enhancement with spectral broadening, ACS Nano 14 (2020) 13841–13851.
[18] J. Sun, H. Hu, D. Zheng, D. Zhang, Q. Deng, S. Zhang, H. Xu, Light-emitting plexciton: exploiting plasmon–exciton interaction in the intermediate coupling regime, ACS Nano 12 (2018) 10393–10402.
[19] D. Zheng, S. Zhang, Q. Deng, M. Kang, P. Nordlander, H. Xu, Manipulating coherent plasmon–exciton interaction in a single silver nanorod on monolayer WSe_2, Nano Lett. 17 (2017) 3809–3814.
[20] M.-E. Kleemann, R. Chikkaraddy, E.M. Alexeev, D. Kos, C. Carnegie, W. Deacon, A. C. de Pury, C. Große, B. de Nijs, J. Mertens, A.I. Tartakovskii, J.J. Baumberg, Strong-coupling of WSe_2 in ultra-compact plasmonic nanocavities at room temperature, Nat. Commun. 8 (2017) 1296.
[21] L. Liu, L.Y. Tobing, X. Yu, J. Tong, B. Qiang, A.I. Fernández-Domínguez, F. J. Garcia-Vidal, D.H. Zhang, Q.J. Wang, Y. Luo, Strong plasmon–exciton interactions on nanoantenna array–monolayer WS_2 hybrid system, Adv. Opt. Mater. 8 (2020) 1901002.
[22] B. Li, S. Zu, Z. Zhang, L. Zheng, Q. Jiang, B. Du, Y. Luo, Y. Gong, Y. Zhang, F. Lin, B. Shen, X. Zhu, A.P. M., Z. Fang, Large Rabi splitting obtained in $Ag\text{-}WS_2$ strong-coupling heterostructure with optical microcavity at room temperature, Opto-Electronic Adv., 2 (2019) 190008.
[23] T. Wu, C. Wang, G. Hu, Z. Wang, J. Zhao, Z. Wang, K. Chaykun, L. Liu, M. Chen, D. Li, S. Zhu, Q. Xiong, Z. Shen, H. Gao, F.J. Garcia-Vidal, L. Wei, Q.J. Wang, Y. Luo, Ultrastrong exciton-plasmon couplings in WS_2 multilayers synthesized with a random multi-singular metasurface at room temperature, Nat. Commun. 15 (2024) 3295.
[24] S. Wang, T. Raziman, S. Murai, G.W. Castellanos, P. Bai, A.M. Berghuis, R. H. Godiksen, A.G. Curto, J. Gómez Rivas, Collective Mie exciton-polaritons in an atomically thin semiconductor, J. Phys. Chem. C 124 (2020) 19196–19203.
[25] K. As' ham, I. Al-Ani, M. Alaloul, S. Abdo, A. Abdulghani, W. Lei, H.T. Hattori, L. Huang, A.E. Miroshnichenko, Enhanced strong coupling in the hybrid dielectric-metallic nanoresonator and WS_2 monolayer, Phys. Rev. Appl., 19 (2023) 054049.
[26] F. Deng, H. Huang, J.-D. Chen, S. Liu, H. Pang, X. He, S. Lan, Greatly enhanced plasmon–exciton coupling in $Si/WS_2/Au$ nanocavities, Nano Lett. 22 (2021) 220–228.
[27] I.A. Al-Ani, K. As' Ham, M. Alaloul, L. Xu, H.T. Hattori, L. Huang, A.E. Miroshnichenko, Quasibound states in continuum-induced double strong coupling in perovskite and WS_2 monolayers, Phys. Rev. B, 108 (2023) 045420.
[28] R. Verre, D.G. Baranov, B. Munkhbat, J. Cuadra, M. Käll, T. Shegai, Transition metal dichalcogenide nanodisks as high-index dielectric Mie nanoresonators, Nat. Nanotechnol. 14 (2019) 679–683.
[29] E. Maggiolini, L. Polimeno, F. Todisco, A. Di Renzo, B. Han, M. De Giorgi, V. Ardizzone, C. Schneider, R. Mastria, A. Cannavale, M. Pugliese, L.D. Marco, A. Rizzo, V. Maiorano, G. Gigli, D. Gerace, D. Sanvitto, D. Ballarini, Strongly enhanced light–matter coupling of monolayer WS_2 from a bound state in the continuum, Nat. Mater. 22 (2023) 964–969.

[30] K. Koshelev, S. Sychev, Z.F. Sadrieva, A.A. Bogdanov, I. Iorsh, Strong coupling between excitons in transition metal dichalcogenides and optical bound states in the continuum, Phys. Rev. B 98 (2018) 161113.
[31] I.A. Al-Ani, K. As' Ham, L. Huang, A.E. Miroshnichenko, H.T. Hattori, Enhanced strong coupling of TMDC monolayers by bound state in the continuum, Laser Photonics Rev. 15 (2021) 2100240.
[32] M. Qin, J. Duan, S. Xiao, W. Liu, T. Yu, T. Wang, Q. Liao, Strong coupling between excitons and quasibound states in the continuum in bulk transition metal dichalcogenides, Phys. Rev. B 107 (2023) 045417.
[33] V. Kravtsov, E. Khestanova, F.A. Benimetskiy, T. Ivanova, A.K. Samusev, I.S. Sinev, D. Pidgayko, A.M. Mozharov, I.S. Mukhin, M.S. Lozhkin, Nonlinear polaritons in a monolayer semiconductor coupled to optical bound states in the continuum, Light Sci. Appl. 9 (2020) 56.
[34] L. Zhang, R. Gogna, W. Burg, E. Tutuc, H. Deng, Photonic-crystal exciton-polaritons in monolayer semiconductors, Nat. Commun. 9 (2018) 713.
[35] S. Li, L. Zhou, F. Deng, J. Xiang, M. Panmai, H. Huang, G. Li, J. Chen, S. Lan, Transverse-electric-polarized polaritons propagating in a $WS_2/Si_3N_4/Ag$ heterostructure, Laser Photonics Rev. 16 (2022) 2100457.
[36] S. Lepeshov, M. Wang, A. Krasnok, O. Kotov, T. Zhang, H. Liu, T. Jiang, B. Korgel, M. Terrones, Y. Zheng, Tunable resonance coupling in single Si nanoparticle–monolayer WS_2 structures, ACS Appl. Mater. Interfaces 10 (2018) 16690–16697.
[37] W. Zhang, J.-B. You, J. Liu, X. Xiong, Z. Li, C.E. Png, L. Wu, C.-W. Qiu, Z.-K. Zhou, Steering room-temperature plexcitonic strong coupling: a diexcitonic perspective, Nano Lett. 21 (2021) 8979–8986.
[38] A. Bisht, J. Cuadra, M. Wersall, A. Canales, T.J. Antosiewicz, T. Shegai, Collective strong light-matter coupling in hierarchical microcavity-plasmon-exciton systems, Nano Lett. 19 (2018) 189–196.
[39] S. Li, L. Zhou, M. Panmai, J. Xiang, S. Lan, Magnetic plasmons induced in a dielectric-metal heterostructure by optical magnetism, Nanophotonics 10 (2021) 2639–2649.
[40] H.R. Philipp, Optical properties of silicon nitride, J. Electrochem. Soc. 120 (1973) 295.
[41] Y. Li, A. Chernikov, X. Zhang, A. Rigosi, H.M. Hill, A.M. Van Der Zande, D. A. Chenet, E.-M. Shih, J. Hone, T.F. Heinz, Measurement of the optical dielectric function of monolayer transition-metal dichalcogenides: MoS_2, $MoSe_2$, WS_2, and WSe_2, Phys. Rev. B 90 (2014) 205422.
[42] N.C. Passler, A. Heßler, M. Wuttig, T. Taubner, A. Paarmann, Surface polariton-like s-polarized waveguide modes in switchable dielectric thin films on polar crystals, Adv. Opt. Mater. 8 (2020) 1901056.
[43] R. Gordon, A.G. Brolo, D. Sinton, K.L. Kavanagh, Resonant optical transmission through hole-arrays in metal films: physics and applications, Laser Photonics Rev. 4 (2010) 311–335.
[44] D.G. Baranov, M. Wersall, J. Cuadra, T.J. Antosiewicz, T. Shegai, Novel nanostructures and materials for strong light–matter interactions, ACS Photonics 5 (2018) 24–42.
[45] J. Wen, H. Wang, W. Wang, Z. Deng, C. Zhuang, Y. Zhang, F. Liu, J. She, J. Chen, H. Chen, S. Deng, N. Xu, Room-temperature strong light–matter interaction with active control in single plasmonic nanorod coupled with two-dimensional atomic crystals, Nano Lett. 17 (2017) 4689–4697.
[46] L. Zhao, Q. Shang, M. Li, Y. Liang, C. Li, Q. Zhang, Strong exciton-photon interaction and lasing of two-dimensional transition metal dichalcogenide semiconductors, Nano Res. 14 (2021) 1937–1954.
[47] A.E. Schlather, N. Large, A.S. Urban, P. Nordlander, N.J. Halas, Near-field mediated plexcitonic coupling and giant Rabi splitting in individual metallic dimers, Nano Lett. 13 (2013) 3281–3286.
[48] K. As' ham, I. Al-Ani, L. Huang, A.E. Miroshnichenko, H.T. Hattori, Boosting strong coupling in a hybrid WSe_2 monolayer–anapole–plasmon system, ACS Photonics, 8 (2021) 489-496.
[49] T. Weber, L. Kühner, L. Sortino, A. Ben Mhenni, N.P. Wilson, J. Kühne, J.J. Finley, S.A. Maier, A. Tittl, Intrinsic strong light-matter coupling with self-hybridized bound states in the continuum in van der Waals metasurfaces, Nat. Mater. 22 (2023) 970–976.